Aspects of Soot Dynamics as Revealed by Measurements of Broadband Fluorescence and Flame Luminosity in Flickering Diffusion Flames

KERMIT C. SMYTH,[†] CHRISTOPHER R. SHADDIX,[‡] and DAVID A. EVEREST[§]
Building and Fire Research Laboratory, National Institute of Standards and Technology, Gaithersburg, MD 20899

Numerous investigators have attributed laser-induced broadband fluorescence observed in both rich, premixed flames and in diffusion flames to small polycyclic aromatic hydrocarbons (PAH). However, the wide variety of experimental flame conditions and excitation/detection wavelengths have clouded the interpretation of such measurements, for example, in terms of indicating either the presence of soot precursors or unreactive by-products (or both). This paper presents PAH fluorescence measurements excited at 283.5 nm and detected at 400–447 nm in a series of steady and flickering methane, propane, and ethylene diffusion flames burning at atmospheric pressure in an axisymmetric, coflow configuration. In the flickering flame experiments, acoustic forcing of the fuel rate is used to phase lock the periodic flame flicker close to the natural flame flicker frequency caused by buoyancy-induced instabilities. When compared to our earlier measurements of soot concentrations in the same flames, soot inception in the annular region is found to occur at the interface between the fluorescing PAH and the region of high radical concentrations. Although the peak PAH fluorescence signals and maximum soot concentrations do not occur at the same spatial locations, indirect evidence is presented that the species responsible for PAH fluorescence participate in either soot inception or growth. In contrast to prior suggestions that PAH fluorescence intensities scale with soot concentrations, the relative peak PAH fluorescence signals are observed to be 1.0:9.8:5.4 for the steady methane, propane, and ethylene flames, respectively, whereas the maximum soot levels follow a different trend of 1.0:19:39. Similar results are observed in the flickering flames, all of which exhibit enhanced PAH fluorescence signals compared to the steady flames. PAH fluorescence excited at 560.3 nm in the steady flames is also strongest for propane. Measurements of flame radiation arising from soot particles have also been made, with detection at 395–547 nm and to a limited degree at 833–900 nm. Visible flame emission is particularly sensitive to the local soot temperature. Comparison of the luminosity images with those of OH· fluorescence and soot scattering shows that the luminosity is strongest where the hydroxyl radicals and soot layers overlap, i.e., in regions of active soot oxidation.

INTRODUCTION

Diffusion flames burning gases, liquids, and even solid fuels often exhibit a natural flame flicker arising from buoyancy-induced flow instabilities which lead to the formation of strong, external vortex rings [1, 2]. These time-varying flames involve different combinations of residence time, temperature, stoichiometry, and strain rate than are commonly found in steady flames, and as such they can serve as important tests of current descriptions of diffusion flame structure, which are based largely on steady flame investigations. Little is known, for example, about the effect of periodic oscillations and the accompanying vortex structures on the chemical and thermal fields within diffusion flames or on flame emissions. The slow rates of aromatic hydrocarbon formation and soot inception and growth [3], which render the concentrations of aromatics and soot independent of mixture fraction [4–8], might be expected to result in a strong sensitivity of these quantities to the flowfield dynamics present in time-varying flames. Indeed, our studies of methane, propane, and ethylene diffusion flames have revealed enhanced soot production for flickering conditions relative to steady flames burning with the same mean fuel and air flow rates [9–12]. The observed increases in the soot concentration are found to be inversely related to a given fuel's sooting tendency [12].

[†] Corresponding author.
[‡] National Research Council NIST Postdoctoral Research Associate, 1993–1995. Present address: Combustion Research Facility, Sandia National Laboratories, Livermore, CA 94551.
[§] National Research Council NIST Postdoctoral Research Associate, 1994–1996. Present address: The University of Michigan, Department of Mechanical Engineering and Applied Mechanics, 2042 G.G. Brown Bldg., Ann Arbor, MI 48109-2125.

COMBUSTION AND FLAME 111: 185–207 (1997)

Published by Elsevier Science Inc.

0010-2180/97/$17.00
PII S0010-2180(97)00017-5

To complement our earlier results on soot production in flickering diffusion flames, this paper presents imaging measurements of laser-induced broadband fluorescence, which has been widely attributed to polycyclic aromatic hydrocarbons (PAH) and often linked to soot inception. Images of visible flame luminosity have also been obtained, which give insight into soot oxidation processes. In contrast to the numerous reports of broadband fluorescence, little attention has been previously devoted to the use of luminosity images beyond simple indication of flame shape. The combination of broadband fluorescence and flame luminosity measurements provides information at both early and late times in the evolution of the soot field for steady and flickering hydrocarbon diffusion flames.

MEASUREMENTS OF LASER-INDUCED BROADBAND FLUORESCENCE

In the 1970s, the first measurements of soot properties were made using laser methods. These early experiments were carried out in premixed flames with visible light (typically 488.0 and 514.5 nm from Ar^+ lasers) and revealed both large scattering depolarization and broadband fluorescence in the soot inception region [13–16], as well as the expected particle extinction and scattering signatures at later residence times. High molecular weight hydrocarbons, possibly soot precursors, were identified as the species responsible. Despite many observations of laser-induced broadband fluorescence over the years, the identity of the fluorescing species and the utility of the observed fluorescence has remained the subject of considerable study and debate.

Role in Flame Chemistry

Broadband fluorescence would be most useful for combustion diagnostics if the emitting species were in fact soot precursors. At elevated temperatures many possible classes of molecules can absorb and emit light in the visible and near-UV regions, including single-ring aromatics (such as the benzyl radical), polycyclic aromatics, polyenes, and polyynes. All of these species have been detected in flame studies [4, 17–20]. Evidence from combined optical and sampling measurements indicates that polycyclic aromatics are the dominant contributors to broadband fluorescence excited at either visible or near-UV wavelengths. Prado et al. [21] found a good correlation between the fluorescence intensity and PAH concentration profiles, while Beretta et al. [22] observed that their PAH fraction gave much stronger fluorescence than other classes of molecules sampled from premixed and diffusion flames. On the basis of those studies, the laser-induced broadband fluorescence measurements presented here will be described as PAH fluorescence.

Prior work has shown that the PAH fluorescence is observed at earlier times than scattering from soot particles for both premixed and diffusion flame conditions. The occurrence of this fluorescence parallels observations of continuum absorption made in the visible and near-UV spectral regions [15, 16, 23–33], and is likely to arise from similar groups of molecules. PAH fluorescence is typically found only under sooting conditions in premixed flames [15, 22, 30, 34], while in diffusion flames there is often a close proximity in the spatial locations of the PAH fluorescence and the soot scattering profiles [4, 21, 22, 35–38]. However, the link between soot precursors and the fluorescing species is not clear, since reactive molecules should exhibit relatively low concentrations, while unreactive by-products will accumulate. In addition, a given PAH molecule can participate in soot formation under favorable conditions of temperature and stoichiometry, whereas under other circumstances the same species will either oxidize or not be chemically active. Several investigators have concluded that the PAH fluorescence observed in their flames arises from stable by-products [15, 22, 30] or that the PAH species detected in sampling studies are unreactive [39–42]. In contrast, other studies have linked the PAH fluorescence to soot precursor molecules based upon circumstantial evidence such as the spatial location of the fluorescence signal and its temporal evolution relative to the soot field [4, 15, 21, 22, 36–38, 43, 44]. Several sampling investigations have also reached the same conclusion [17, 45–48].

A further complication in interpreting PAH fluorescence signals is the observation that the fluorescence measured as a function of flame position arises from a group of molecules whose composition changes with time [15, 49]. That is, the relative concentration of the various PAH species evolves within the flame. Nevertheless, numerous studies have established that this broadband fluorescence is an indicator of conditions conductive to soot formation, as described by Kennedy [50]:

> The identity of the fluorescent species in sooting diffusion flames can not be determined unequivocally, and it is by no means certain that these species are active participants in the soot particle inception process. Nevertheless, it is reasonable to assume that the fluorescent species are at least by-products of the particle formation chemistry, and as a result they are indicators of the rate of the main soot particle formation chemistry.

Polycyclic aromatic hydrocarbons have long been identified as attractive candidates for soot precursors, both as fundamental building blocks and, more recently, as species which participate in reactive coagulation leading to soot inception [47, 48, 51–54]. McKinnon and Howard [47] and Marr et al. [52] have also argued that PAH are important in surface growth, especially those containing two to four rings [52].

Spectral Characteristics

Most investigations of laser-induced PAH fluorescence have reported spectra which exhibit a single maximum and show no discernible structure, using excitation with either visible or UV radiation. The spectral shapes are found to be closely similar for flames burning simple hydrocarbon fuels [55, 56] as well as those of kerosene, gasoline, and iso-octane–naphthalene [57], polystyrene and polymethylmethacrylate (PMMA) [58, 59], and pyridine [15]. In addition, the probe-sampling results of Toqan et al. [60] showed that the same PAH molecules are present in both premixed laminar flames and turbulent diffusion flames. These findings suggest that a common group of aromatics is formed for different fuels and combustion conditions.

In contrast to the broad, featureless spectra reported previously, several studies have described structured fluorescence for visible [16, 21, 29, 49, 56, 61, 62] and UV [19, 43, 49, 56, 63] excitation. This has encouraged attempts to identify specific peaks with particular aromatic compounds, usually containing two to four rings, such as acenaphthalene [19, 49, 56, 61]. Given the lack of high-temperature spectral data and quantum yield information for polycyclic aromatic hydrocarbons [61, 64, 65], these efforts may only be considered a limited success.

EXPERIMENTAL APPROACH

Unconfined laminar diffusion flames were stabilized on a co-annular burner consisting of a 10.2-cm diameter air annulus surrounding a 1.1-cm diameter fuel tube, with a loudspeaker attached to the plenum below the fuel tube. As with previous studies [9–12, 66, 67], the optical diagnostics were phase-locked to a sinusoidal oscillation of the fuel stream at the 10-Hz repetition rate of a Nd^{3+}:YAG laser, permitting phase-specific measurements to be performed in the time-varying flow fields. Figure 1 shows a schematic of the burner and phase-locked imaging setup. A synthesized function generator provided exact reproducibility of the flickering flame forcing amplitude and the detection phase settings. All conditions were identical to our recent investigation of soot production in flickering methane, propane, and ethylene diffusion flames [12]. The mean fuel flows were set such that the flow rate of carbon atoms was approximately the same for each fuel, with area-averaged fuel velocities of 7.8, 2.6, and 4.1 cm/s and visible flame heights of 79, 85, and 91 mm for the methane, propane, and ethylene steady flames, respectively. None of these steady flames emits smoke. Air coflow velocities were 7.9 cm/s for the methane flame and 8.7 cm/s for the propane and ethylene flames.

Measurements were performed on the three different steady flames and for both moderately and vigorously flickering conditions produced by applying sine waves of magnitude 0.75 and 1.5 V (peak-to-peak) to the plenum loudspeaker. In addition to our soot measurements in these flames [10, 12], prior studies have reported OH· concentrations in the

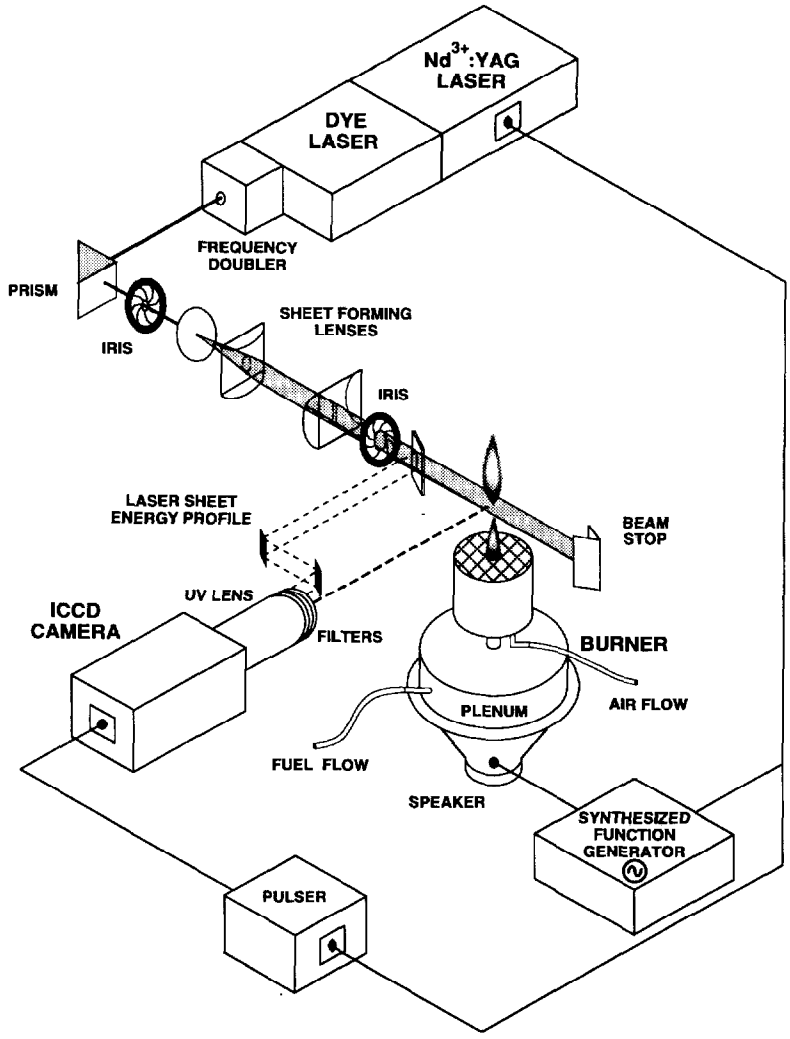

Fig. 1. Experimental setup for two-dimensional imaging of axisymmetric diffusion flames which are acoustically excited and phase locked to the pulsed dye laser system operating at 10 Hz. Images are recorded using an intensified charge-coupled device (ICCD) camera.

steady methane flame and in a slightly shorter (fuel flow velocity of 4.0 cm/s, termed non-smoking or NS) ethylene flame [68], as well as CO concentrations [66] and temperature profiles [67] in the steady and flickering methane flames. Most recently, Zhang and Megaridis [69] have compared the primary soot particle diameters in the steady and strongly flickering methane flames.

Laser-Induced PAH Fluorescence

PAH fluorescence was excited at a wavelength of 283.5 nm and detected at 90° to the propagation direction of the laser beam on an intensified charge-coupled device (CCD) camera using a short-pass dielectric filter with a bandpass of 400–447 nm (50% transmission points) and an f/4.5 100-mm focal length UV lens. This relatively narrow bandpass was used to discriminate against flame luminosity from the soot particles. With the polarization of the incoming UV radiation horizontal relative to the detection axis, elastic scattering from the soot particles was undetectable. In an earlier investigation [4], spectrally resolved scans of the PAH fluorescence excited at 282 nm revealed no contributions from molecular species,

such as C_2, in this bandpass. The images shown here for the flickering flames typically were collected by accumulating three successive laser shots on the CCD array, thus improving the signal-to-noise ratio compared to single-shot measurements while minimizing the effects of flame movement. Binning the pixels by 3 in each direction gave an effective spatial resolution of 250 μm per data point with the 3.8:1 imaging optics. Sufficiently stable conditions existed in the steady flames and at the lowest height in the flickering flames that 30-shot averages were taken. Shot-to-shot spatial profiles of the laser energy were recorded via on-camera imaging of a reflection from the incident laser sheet (see Fig. 1). This information was used to account for the variation in light intensity along the sheet (see below), after background and flat-field corrections had been applied to each image.

A limited number of measurements of visible PAH fluorescence were also made in the steady propane and ethylene flames. For these images the incoming beam at 560.3 nm was vertically polarized, and a detection bandpass of 590–659 nm (50% transmission points) was obtained using two glass filters. A polarization filter oriented to pass only horizontally polarized light discriminated against particle scattering. Visible PAH fluorescence was not observed in the steady methane flame under these experimental conditions, which involved pulsed laser excitation and detection. In our prior investigation with continuous-wave excitation (at 488 nm) and lock-in detection, visible PAH fluorescence was observable in a methane/air diffusion flame [4].

Earlier work from this and other laboratories has found that both the emission spectra and the spatial location of the maximum PAH fluorescence signals in diffusion flames depend upon the excitation and detection wavelengths. For shorter excitation wavelengths in the visible and UV regions, the fluorescence emission becomes stronger and its wavelength of maximum intensity shifts to the blue relative to longer wavelength excitation [16, 35, 49, 56, 62]. In addition, for longer detection wavelengths the location of the strongest PAH fluorescence signal generally shifts closer to the high-temperature reaction zone in the fuel-rich region of diffusion flames [21, 49, 70]. Longer wavelength detection thus favors the observation of PAH fluorescence at higher temperatures just to the rich side of the stoichiometric position in hydrocarbon diffusion flames.

Broad, structureless spectra have been observed in our prior investigations of PAH fluorescence in both premixed flames (unpublished results) and in diffusion flames using visible and ultraviolet excitation wavelengths [4, 62].[1] Of particular interest for the present study are our earlier observations in a CH_4/air diffusion flame [4], where fluorescence profiles obtained using UV radiation at 282 nm showed evidence for two populations at early times (i.e., at low heights above the burner). These components could be distinguished by their spatial locations and to a limited degree by the wavelength of their emission. One feature followed a constant-temperature contour with increasing height above the burner and coincided with the region of soot inception, suggesting that the fluorescing species were associated with soot formation. In contrast, the position of the second peak simply tracked the convective streamlines into cooler and richer flame regions and its intensity grew with height above the burner, apparently indicating that this second fluorescence component arose from unreactive by-products. In addition, Smyth et al. [4] measured PAH fluorescence with visible excitation at 488 nm; the resulting profiles detected at 510 nm were located close to the soot inception region. Beretta et al. [22] also found that a feature detected at UV wavelengths in a CH_4/O_2 diffusion flame was not connected to soot formation, while they attributed a visible feature to species involved in soot inception.

For the present study, additional measurements of PAH fluorescence were made in a CH_4/air diffusion flame supported on a rectilinear Wolfhard–Parker burner. The presence of two components in the profiles was con-

[1] A structured fluorescence spectrum was detected in a CH_4/O_2 diffusion flame by Miller et al. [62], but only when a stabilization plate was positioned close to the burner surface. Under these conditions considerable recirculation of combustion gases and particles occurred.

firmed for excitation at 283.5 nm. In addition, longer wavelength detection was found to favor observation of the PAH feature which is located in the soot inception region, as opposed to the component found at richer and cooler flame positions. These results were compared with imaging measurements in the axisymmetric CH_4/air diffusion flame, using the same excitation wavelength and short-pass dielectric filters along with the intensified CCD camera. The images obtained in the axisymmetric diffusion flames emphasized the high-temperature (and thus more interesting) PAH component, which is closely linked to soot inception.

Prior to the imaging experiments the laser energy dependence of the PAH fluorescence was measured. Signals were linear at low laser intensities but were too weak to obtain single-shot images with a reasonable signal-to-noise ratio. Extending the detection bandpass to longer wavelengths (such as 500 nm) resulted in interference from luminosity. At high laser intensities, laser-induced incandescence produced strong signals from the soot particles [10, 12]. For intermediate laser energies the PAH fluorescence exhibited evidence of partial optical saturation for intensities slightly lower than that required for partial saturation of the $S_{21}(8)$ transition in the OH· $A^2\Sigma^+ \leftarrow X^2\Pi_i$ (1,0) band. Measurements of the PAH fluorescence were made using laser intensities in this intermediate regime (peak intensity $\approx 1 \times 10^7$ W/cm^2 in a bandwidth of 0.4 cm^{-1}), with care taken to avoid laser excitation of incandescence from the soot particles. Note that fully saturated fluorescence signals could not be obtained using our intensified CCD camera, since its minimum gate width of 19 ns is far longer than the laser pulse duration of $\sim$ 5 ns. Thus, even if the detection optics are configured such that the spatial wings of the laser sheet do not contribute significantly to the observed PAH fluorescence, the low-intensity leading and trailing temporal portions of the beam will produce measurable linear signals. In the images presented here the observed laser-induced PAH fluorescence was measured with an 85-ns gate, and the signals were corrected using an $I^{1/2}$ intensity dependence.

Flame Luminosity

Visible radiation from the soot particles was measured using a wide 3-μs gate on the intensified CCD camera and a short-pass dielectric filter (395–547 nm bandpass for transmission $\geq$ 50%). These luminosity signals arise from all regions of the flame containing soot, unlike the images of PAH fluorescence (and earlier work on OH· fluorescence and soot scattering [9–12]) excited using a two-dimensional laser sheet. However, most of the luminosity is collected from the image plane at the flame centerline defined by the f/4.5 collection optics with a nominal depth of field of $\pm$2 mm.

Luminosity measurements were also made at near-IR wavelengths using a long-pass filter with 50% transmission at 833 nm; the intensified CCD camera detects light to 900 nm. This bandpass transmits nearly the identical fraction of the total soot radiation (approximately 1 part in 8000) as the visible bandpass for a temperature of 1800 K. The near-IR images are compared with the visible results in the next section and discussed in terms of the total soot radiation. Even if the total radiation were accurately measured, it would not, of course, faithfully reflect soot concentrations, due to the strong temperature dependence of soot emission. Despite the qualitative nature of the luminosity measurements, they serve as a sensitive indicator of high-temperature soot, especially when detecting visible flame emission.

OH· Fluorescence and Soot Scattering

The spatial locations of the PAH fluorescence and visible flame luminosity observed in the present study can be compared with our earlier two-dimensional images of OH· fluorescence and soot scattering [9–12]. OH· fluorescence marks the high-temperature reaction zone, while the earliest soot scattering signal indicates the region of soot inception. For these measurements the laser wavelength was tuned to 283.55 nm, corresponding to excitation of the $Q_1(8)$ line of the $A^2\Sigma^+ \leftarrow X^2\Pi_i$ (1,0) band of OH·. Excitation from the $N'' = 8$ level minimizes the Boltzmann population correction for temperature variations (less than 5% over

the range 1400–2100 K [71]). Filter combinations with differing UV cut-on wavelengths were employed to vary the attenuation of the soot scattering signals, whose peak levels vary by more than a factor of 300 for the different fuels [12].

RESULTS

PAH Fluorescence

Figure 2 qualitatively compares the early time development in the steady methane, propane, and ethylene flames by presenting surface plots of simultaneous OH· fluorescence, soot scattering, and UV PAH fluorescence. The OH· fluorescence occurs farthest from the burner centerline, while the soot scattering is apparent as a sharp ridge just inside the OH· fluorescence region and PAH fluorescence is widely distributed in the fuel-rich region. Identical detection filters were used for the propane and ethylene flames, whereas a filter which transmitted more of the scattering signal was utilized for the low-sooting methane flame. The actual OH· concentrations in these steady flames are the same to within approximately $\pm 5\%$ at $H = 7$ mm above the burner [68, 72].

Figure 3 presents two-dimensional images in the steady flames which show PAH fluorescence alongside images of OH· and soot scattering. Selected profiles from these images are overlaid in Fig. 4, clearly displaying the relative spatial location of the OH·, soot scattering, and PAH fluorescence. Several features are evident in these figures:

1. PAH fluorescence appears earliest (i.e., at the lowest height above the burner) for ethylene, the most heavily sooting fuel investigated here. In the lightly sooting methane flame the PAH fluorescence is much weaker

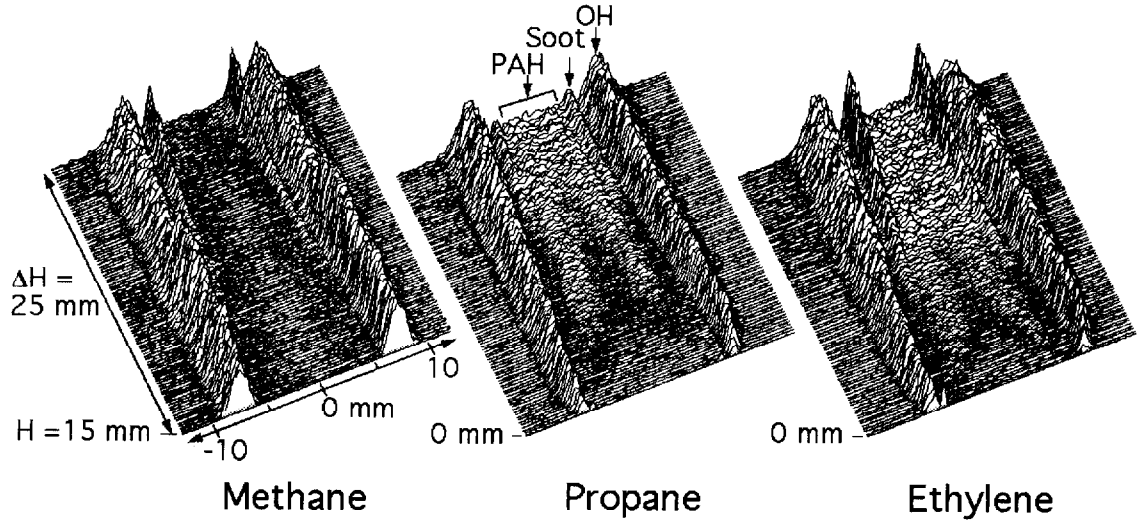

Fig. 2. Surface plots of OH· fluorescence (farthest from the burner centerline), soot scattering (apparent as a sharp ridge just inside the OH· fluorescence region), and PAH fluorescence (widely distributed in the fuel-rich region) in the steady methane, propane, and ethylene flames. Each plot shows a flame portion 25 mm wide by 25 mm high. In these plots the maximum OH· signals have been scaled to a common value at $H = 7$ mm. The excitation wavelength of 283.55 nm coincides with the $Q_1(8)$ line of the $A^2\Sigma^+ \leftarrow X^2\Pi_i$ (1,0) band of OH·. Identical detection filters (Schott WG295*, Hoya UV28, and Hoya U340) were used for the propane and ethylene flames, whereas only the Hoya U340 filter was utilized for the low-sooting methane flame in order to transmit more of the soot scattering signal.

* Certain commercial products and equipment are identified herein in order to adequately specify the experimental procedure. Such identification does not imply recommendation by the National Institute of Standards and Technology, nor does it imply that this equipment is the best available for the purpose.

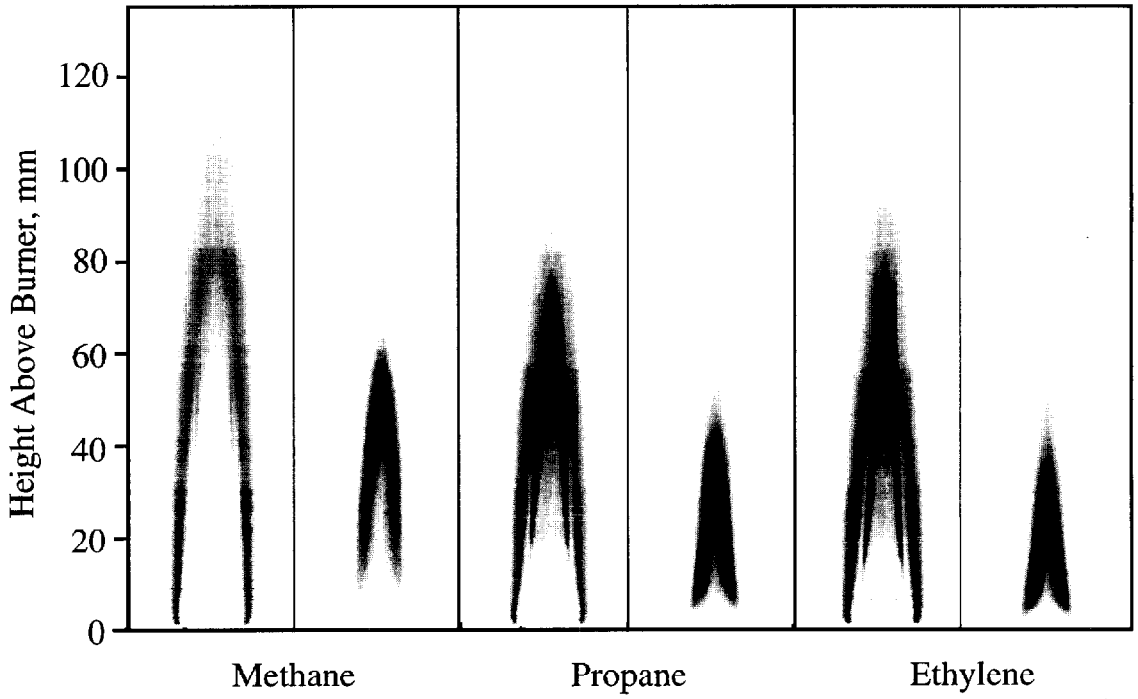

Fig. 3. Two-dimensional images in the steady methane, propane, and ethylene flames of OH· and soot scattering (left panel for each fuel; from Ref. 12, Fig. 9) compared to PAH fluorescence (right panel, present work; excitation at 283.5 nm and detection at 400–447 nm). The scaling for the methane PAH fluorescence image is 10 × more sensitive than for propane and ethylene. Filters used for detecting the OH· and soot scattering signals were Hoya UV28 and U340 for methane; Schott WG280, Hoya UV28, and Hoya U340 for propane; Schott WG295 and Hoya U340 for ethylene. Relative peak PAH fluorescence intensities are given in Table 1, and absolute soot scattering intensities are reported in Ref. 12.

compared to propane and ethylene (note that the methane PAH fluorescence signals have been multiplied by 10 in Figs. 3 and 4; see also Table 1).

2. Soot scattering appears at the high-temperature edge of the PAH fluorescence profile for all of the flames. The location of soot inception is revealed by the earliest scattering signals and occurs at the interface between high radical concentrations (indicated by the OH· profile) and high aromatic concentrations (marked by the PAH fluorescence profile). This description of soot inception conditions is identical to that presented in our prior mass spectrometric and optical studies of a CH_4/air diffusion flame [4]. Shaddix and Smyth also reported more sensitive soot scattering measurements in these flames using vertically polarized visible light [12]; the radial locations of the peak signals are identical to the UV, horizontally polarized scattering results [9].
3. The spatial locations of the maximum PAH fluorescence and the soot scattering signals do not coincide. Since the convective streamlines in these axisymmetric flames carry the aromatic molecules toward the burner centerline [73] and the PAH diffusion velocities are low [74], it is unlikely that at early times most of the fluorescing species can directly participate in soot inception and growth. However, some diffusion of the PAH toward higher temperatures occurs at higher heights (the inward horizontal velocities decrease with height above the burner surface [75]), and soot inception eventually takes place on the centerline for all of the flames [12; see Figs. 10 and 11 below].

Table 1 compares the maximum PAH fluorescence signals observed in the steady and flickering methane, propane, and ethylene flames. Also shown are the peak soot volume fractions obtained from our laser-induced in-

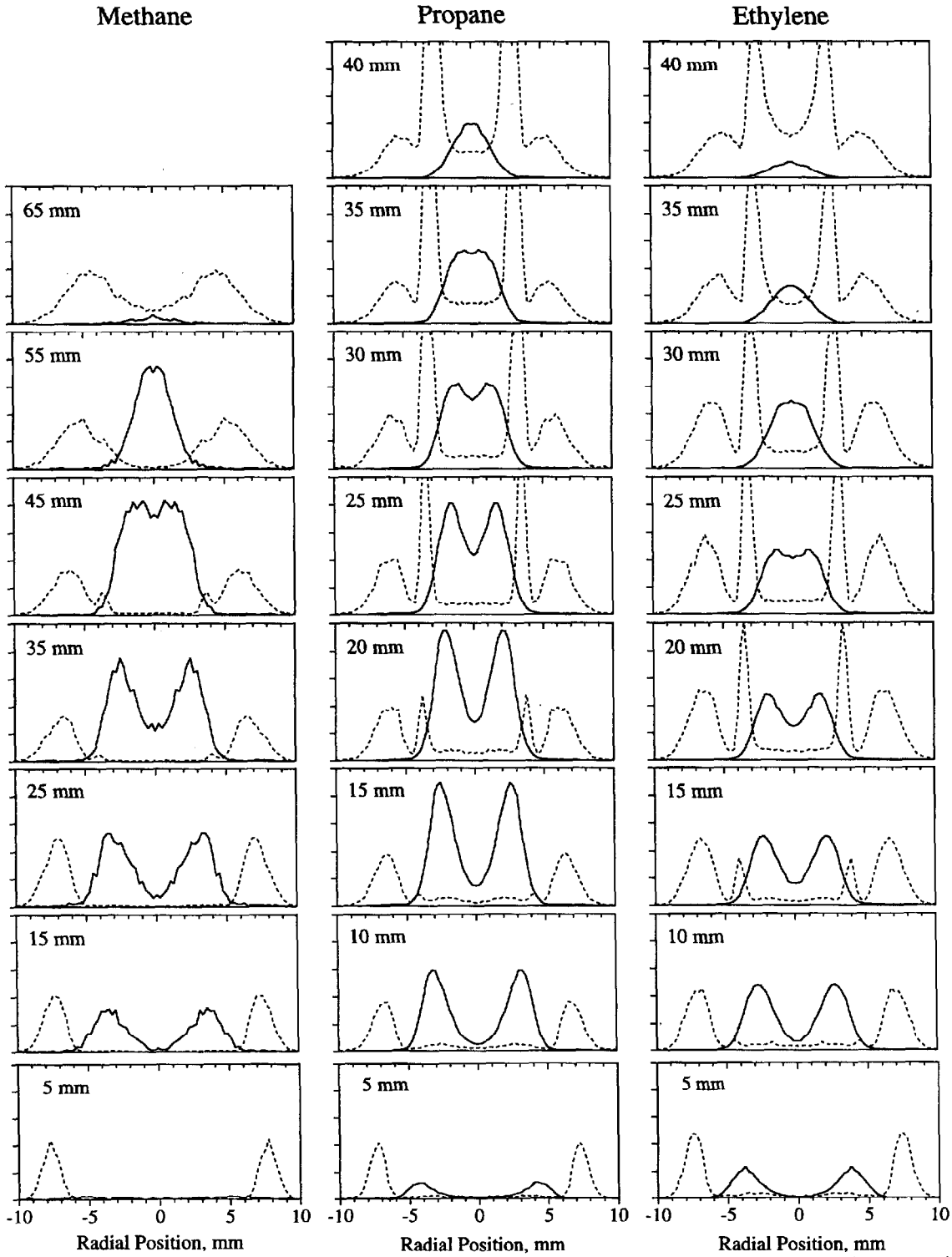

Fig. 4. Selected profiles from Fig. 3 comparing PAH fluorescence (solid lines) with OH· and soot scattering (dotted lines) for the steady methane, propane, and ethylene flames. The scaling for the methane PAH fluorescence profiles is 10 × more sensitive than for propane and ethylene. Relative peak PAH fluorescence intensities are given in Table 1, and absolute soot scattering intensities are reported in Ref. 12.

TABLE 1

PAH Fluorescence and Soot Concentrations in Steady and Flickering Flames

Fuel	Peak PAH Fluorescence[a] Excitation at 283.5 nm			Peak Soot Volume Fraction[b] f_v ($\times 10^{-6}$)		
	Steady Flame	Moderately Flickering Flame	Strongly Flickering Flame	Steady Flame	Moderately Flickering Flame	Strongly Flickering Flame
Methane	1.0	3.9	3.9	0.33	1.8	2.0
Propane	9.8	18	26	6.3	10	8.5
Ethylene	5.4	12	21	13	20	18

[a] Estimated uncertainties in the relative PAH fluorescence signals are ±20% for methane and ±10% for propane and ethylene.

[b] Values from Shaddix and Smyth [12].

candescence measurements [12]. For the steady flames, propane exhibits the highest PAH fluorescence intensities, followed by ethylene (which has the greatest soot concentration) and then methane. It is also of interest to compare the structure of the PAH images in the three steady flames (Figs. 3 and 4). For methane, the largest signals occur near the top of the flame at the burner centerline. In contrast, propane exhibits the strongest signals in the annular region (H = 20 mm above the burner). Ethylene exhibits the earliest PAH fluorescence signals low in the flame with an intense annular region which quickly fills in to the centerline by H = 25–30 mm; maximum signals are very similar in the annular and centerline regions for H = 10–30 mm. The luminous flame heights in the three steady flames are about the same: 79, 85, 91 mm for methane, propane, and ethylene, respectively. Note that for ethylene, the most heavily sooting fuel, the PAH fluorescence signals first appear and then disappear faster than for propane. Both propane and ethylene exhibit a much more rapid evolution of the PAH fluorescence than methane.

For the PAH fluorescence excited and detected at visible wavelengths, the steady propane flame again was found to exhibit the largest signals, ~ 30% greater than for ethylene. Similar to the results discussed previously, the peak signals in the propane flame were observed in a localized, annular region, while the largest signals in the ethylene flame occurred over an extended area.

Figure 5 presents PAH fluorescence images for the moderately (0.75-V acoustic excitation) and vigorously (1.5-V acoustic excitation) flickering methane, propane, and ethylene flames. Flickering conditions enhance the PAH signals for all fuels, most dramatically for methane (~ 4 ×), followed by propane and ethylene (~ 2 × for moderately flickering and ~ 2.5–4 × for vigorously flickering conditions). The strongest fluorescence signals occur following clip-off in the flickering methane and ethylene flames, whereas for propane the largest signals are found in the annular region just prior to clip-off. For a given level of acoustic excitation, the width of the PAH fluorescence images for the methane flames is considerably greater than for the more heavily sooting propane and ethylene flames. Our OH·/soot scattering images and soot profile measurements [12] also exhibit greater widths for the methane flames. The observed flame widths presumably reflect the differing initial fuel velocities as well as variations in thermal expansion caused by unequal radiation losses from the soot layer. Table 1 shows that the maximum soot concentrations in these flames vary by factors of 9–39 for the three fuels, depending upon the combustion conditions.

Flame Luminosity

Figures 6 and 7 present images of visible flame luminosity (detection bandpass of ~ 395–547 nm) for the steady and flickering methane, propane, and ethylene flames. Only radiation

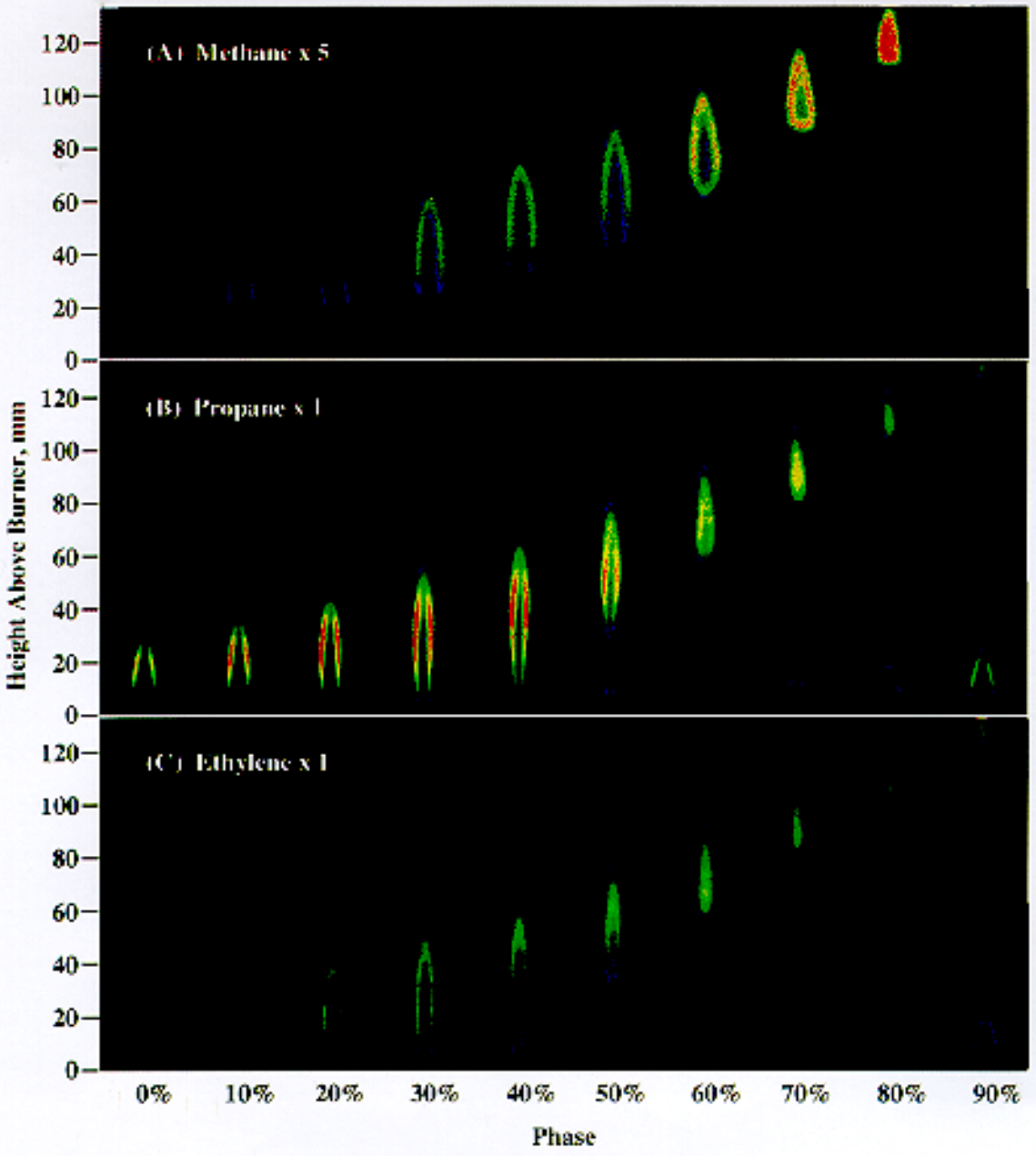

Fig. 5. Two-dimensional images of PAH fluorescence in the (A) methane, (B) propane, and (C) ethylene flames for moderately flickering (left) and vigorously flickering (right) conditions. The scaling for the methane results is 5 × more sensitive than for propane and ethylene; relative peak PAH fluorescence intensities are given in Table 1. The color palette is an 8-bit, 32-color linear scale, with red representing the strongest PAH fluorescence signals and purple–blue indicating the weakest signals. 0% phase is arbitrarily set to show the highest development to the right in the figures.

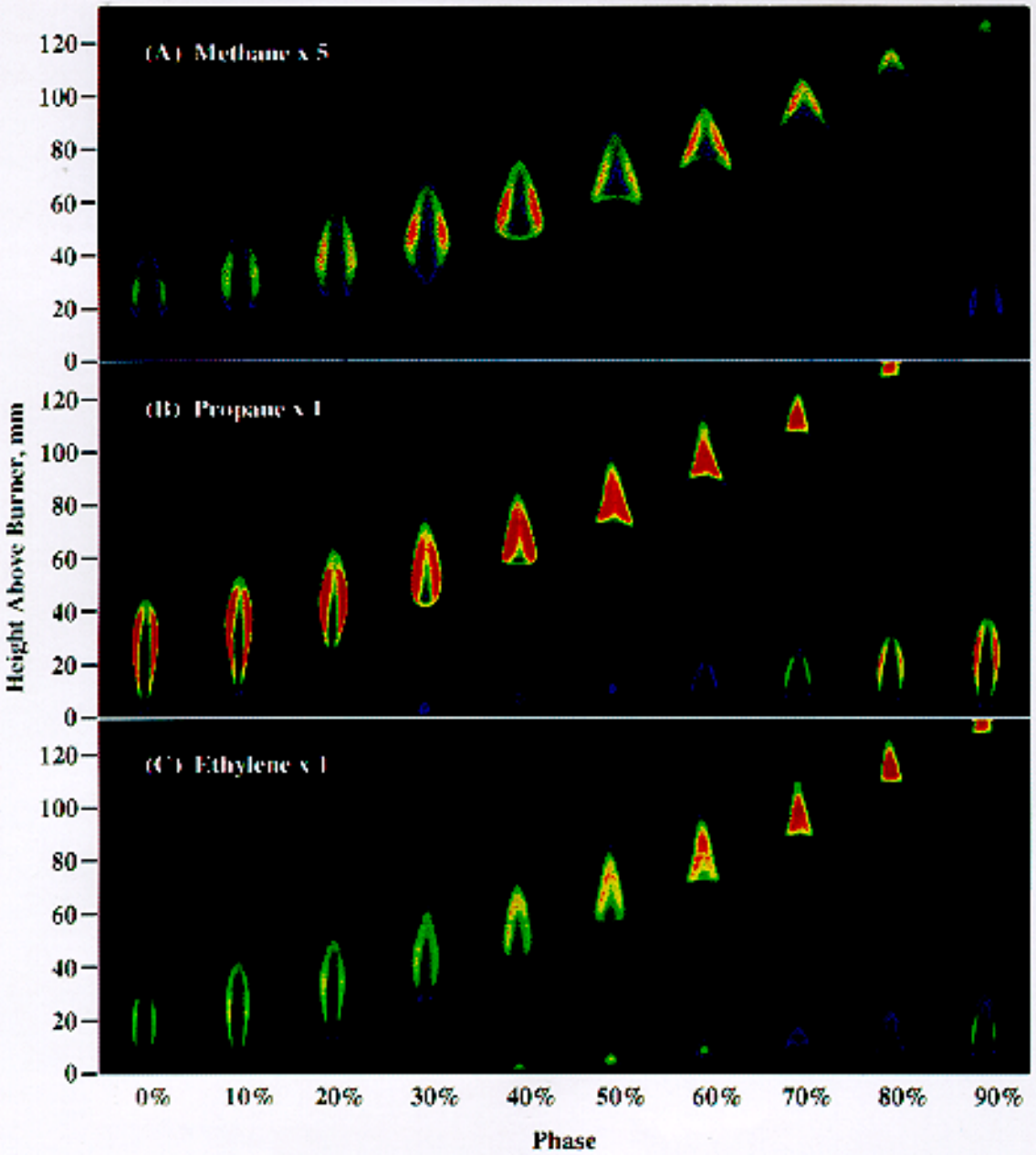
(A) Methane x 5
(B) Propane x 1
(C) Ethylene x 1
Height Above Burner, mm
120
100
80
60
40
20
0
0%
10%
20%
30%
40%
50%
60%
70%
80%
90%
Phase

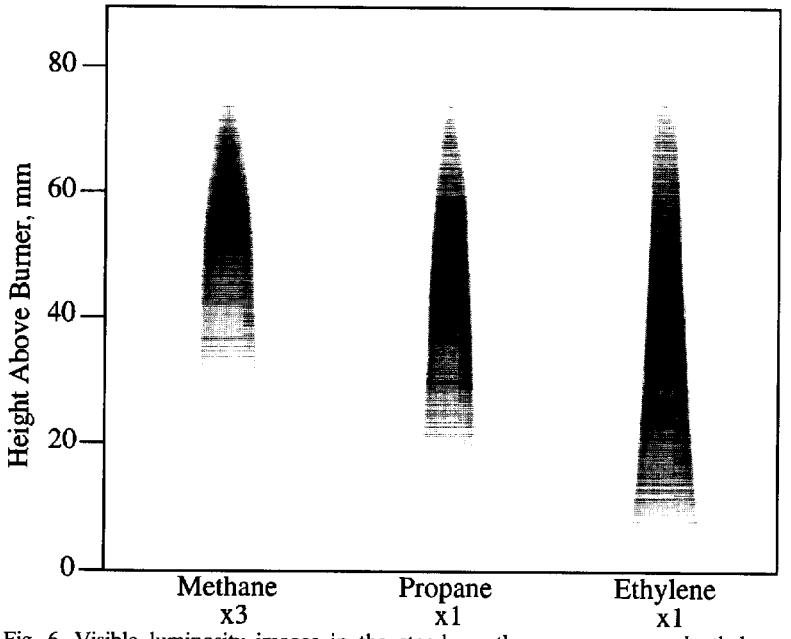

Fig. 6. Visible luminosity images in the steady methane, propane, and ethylene flames obtained with a detection bandpass of 395–547 nm (50% filter transmission). The scaling for the methane results is 3 × more sensitive than for propane and ethylene.

from soot particles is detected in this wavelength region; emission from electronically excited CH· at 431 nm [76] and C_2: at 438, 474, and 517 nm [76] is not observed. For example, no emission from these species is evident at low heights above the burner in the methane flame (Fig. 6), presumably because the soot luminosity is much stronger than molecular emission. The most noticeable aspect of the luminosity results is that the strongest signals generally appear in highly localized regions, especially in the flickering flames. Compared to our measurements of the soot volume fractions and soot scattering signals [9–12; Fig. 3], the luminosity images reveal somewhat different aspects of soot evolution in the steady vs flickering flames. In the steady methane, propane, and ethylene flames, the maximum soot concentrations occur at $H = 65$, 40, and 35 mm above the burner, respectively [12]. Figure 6 shows that the largest methane luminosity signals lie at $H = 55$–70 mm, where soot oxidation is occurring. However, this is not the case for the more heavily sooting propane and ethylene flames, due to increased radiation losses. For example, temperatures are more than 300 K cooler in the upper region of the ethylene flame, at $H = 70$–88 mm above the burner, compared to the methane flame [68]. In the propane and ethylene flames the peak visible luminosity signals occur near the location of the maximum soot levels, i.e., in an annular region at mid-height.

The flickering flames for all three fuels present an interesting contrast, in that intense visible luminosity appears where soot concentrations are small, such as at the clip-off locations and at the tops of the flames which remain attached to the burner. On the other hand, the visible emission is relatively weak where the soot concentrations are highest, typically at mid-height in the clipped flamelets [12]. This lack of correlation between the maximum visible flame luminosity and the peak soot volume fractions arises because the visible luminosity is particularly sensitive to high-temperature soot particles, as illustrated by the computations shown in Fig. 8. Here the emissive power for the total radiation from a blackbody as a function of temperature is compared to that detected in the bandpasses used in the visible luminosity experiments as well as in the

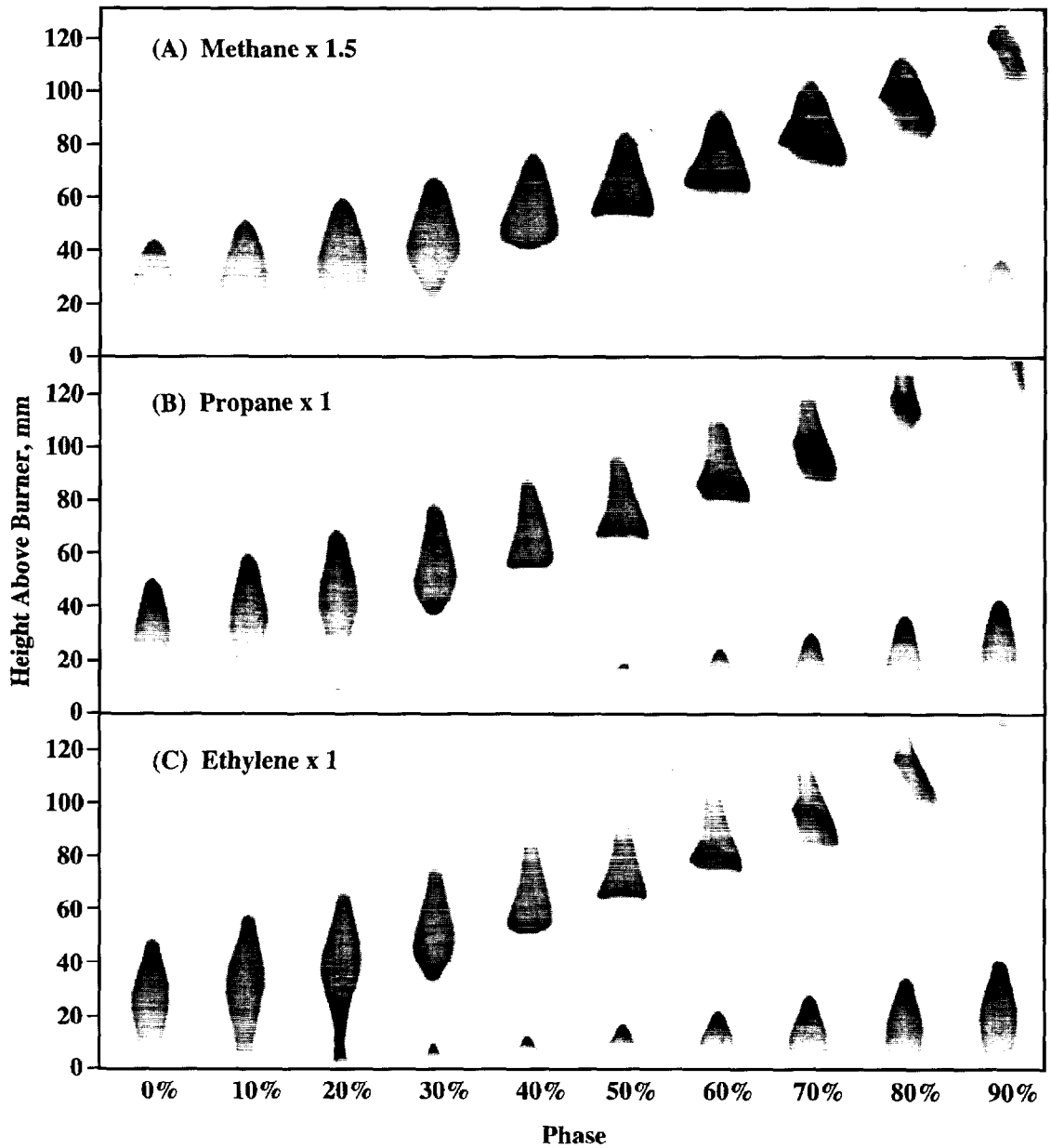

Fig. 7. Visible luminosity images for (A) methane, (B) propane, and (C) ethylene flames obtained under moderately flickering (left) and vigorously flickering (right) conditions with a detection bandpass of 395–547 nm (50% filter transmission). The scaling of the methane results is 1.5 × more sensitive than for propane and ethylene, and the phase settings match those presented in Fig. 5.

limited series of measurements at near-IR wavelengths (833–900 nm). To calculate the respective curves for the visible and near-IR bandpasses, the blackbody emission was multiplied by the actual filter transmission functions and by the CCD cathode sensitivity; all curves were then normalized at 1800 K. For the high temperatures typical of soot oxidation, 1600–1900 K [77], the emission curve for the visible bandpass exhibits a much steeper slope with

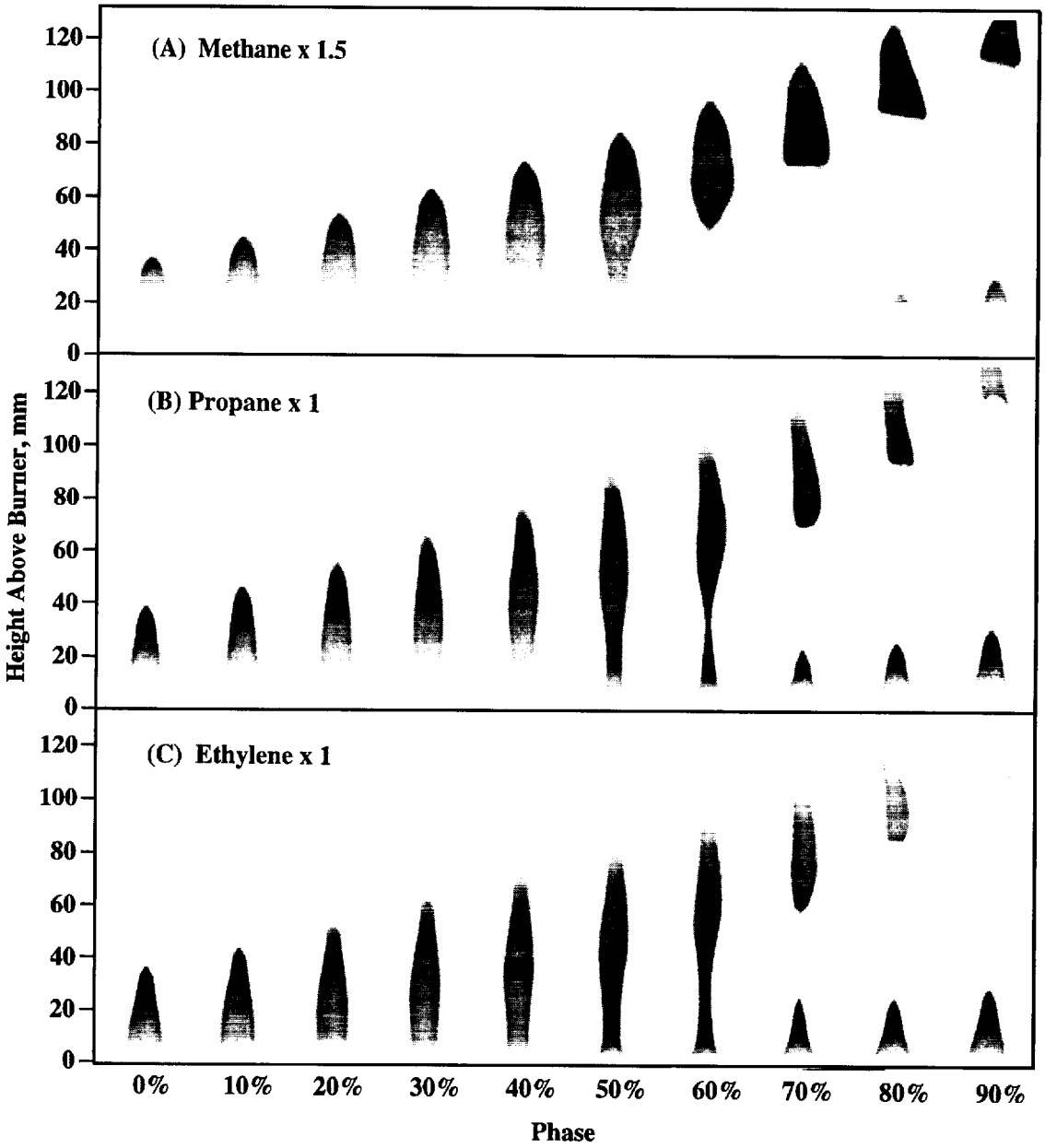

Fig. 7. continued

temperature than that for the total radiation. In other words, the visible emission depends strongly upon the local soot temperature and is not a good indicator of the total soot radiation. An intermediate dependence occurs for the near-IR wavelength detection bandpass (this was the longest wavelength region detectable with our intensified CCD camera). Figure 9 compares selected luminosity images for the steady and flickering ethylene flames at these two detection bandpasses. As expected, more of the soot field is apparent for luminosity

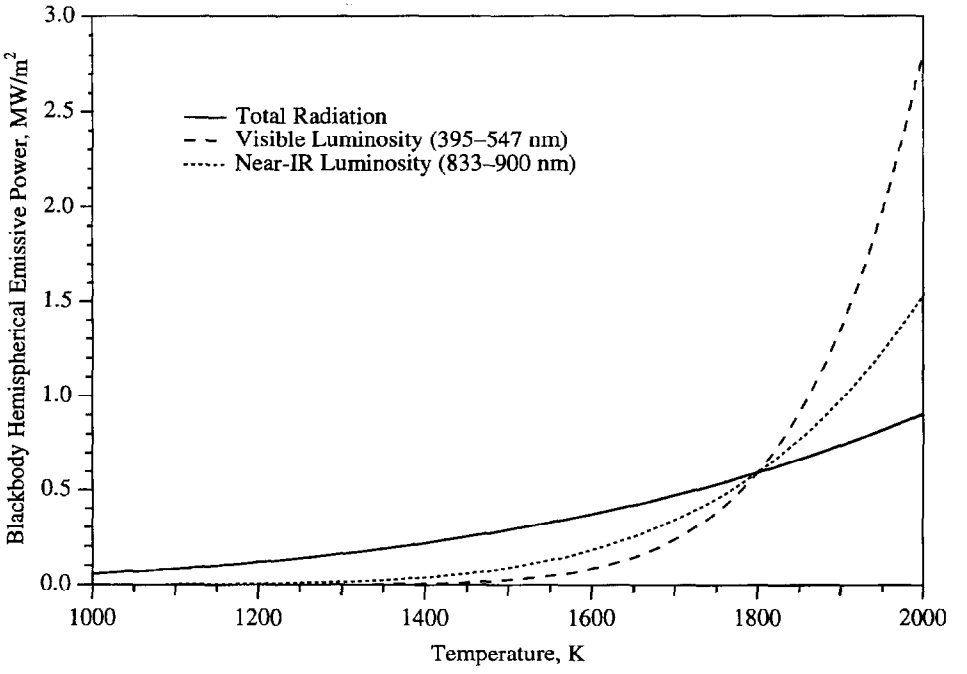

Fig. 8. Computations of the relative temperature response for detection of luminosity with different bandpasses compared to that calculated for the total soot radiation. The actual filter transmission curves multiplied by the CCD cathode sensitivity have been used to determine the temperature response for the visible and near-IR bandpasses. The emissive powers are normalized to the same value at 1800 K for each curve; both bandpasses transmit approximately 1 part in 8000 of the total radiation at this temperature.

detection at near-IR wavelengths, whereas the visible emission is observable only in much more restricted regions.

DISCUSSION

PAH Fluorescence Intensities vs PAH Concentrations

The most striking result of our PAH fluorescence measurements is the observation that the steady and flickering propane flames exhibit peak signals which are consistently stronger (by 25–80%) than the corresponding ethylene flames. In contrast, maximum soot concentrations in the ethylene flames are twice as large as in propane for all of the flames (Table 1). In addition, the visible PAH fluorescence signals in the steady propane flame are ~ 30% stronger than those observed in the steady ethylene flame. Both propane and ethylene are heavily sooting fuels compared to methane [12, Table 1], and both exhibit much stronger PAH fluorescence signals than methane. However, if the overall intensity of PAH fluorescence were a reliable indicator of soot precursor concentrations, then one might anticipate that ethylene would also display the stronger PAH fluorescence, since soot inception is often regarded as the key step in determining soot concentrations [3]. In other words, although the spatial locations of the maximum PAH fluorescence signals and the peak soot volume fractions do not coincide, the PAH fluorescence intensities in the soot inception regions might be expected to track the maximum soot signal levels, at least qualitatively.

Examination of the PAH fluorescence profiles for the steady propane and ethylene flames (Fig. 4) reveals that at $H = 5$ mm the maximum PAH fluorescence signal is largest for ethylene; this flame exhibits a small soot scattering signal by $H = 10$ mm. Soot inception occurs more slowly in propane, where a soot scattering signal does not appear until $H = 15$ mm. Here the PAH fluorescence intensity at

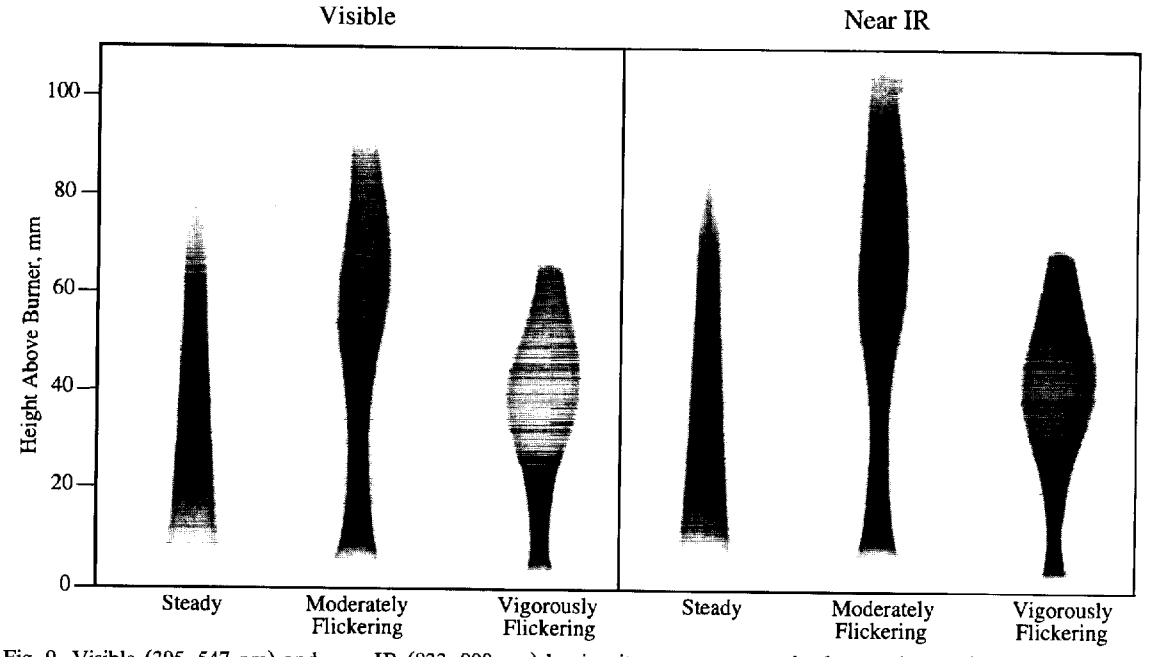

Fig. 9. Visible (395–547 nm) and near-IR (833–900 nm) luminosity measurements in the steady and flickering ethylene flames. For the flickering flames the phases are 60% in the moderately flickering and 20% in the vigorously flickering cases, respectively (Fig. 7).

the radial location of soot inception is very similar to that observed in the ethylene flame (at $H = 10$ mm), but the peak PAH fluorescence signal at richer flame locations is considerably larger. The faster soot production in the ethylene flame may effectively scavenge aromatic species that show up as PAH fluorescence in the propane flame [33]. Thus, no simple picture emerges which relates the intensity of the PAH fluorescence at either the location of soot inception or in terms of peak signal levels to the eventual maximum soot concentrations. Senkan and Castaldi have also found that PAH production does not parallel soot levels in rich premixed flames ($\phi = 2.5$) burning methane, ethane, and propane [78].

It is tempting to associate the PAH fluorescence signal intensities with PAH concentrations. However, several factors must be identical for the relative fluorescence intensities to accurately mirror PAH concentrations in different flames, including the group of molecules being excited, the temperature, and the collisional quenching environment. Both the partition functions of the PAH and the quantum yields of their emission change markedly as a function of position in a hydrocarbon diffusion flame, due to wide variations in the local temperature and chemical composition. The Boltzmann populations of low-lying vibrational levels are particularly sensitive to temperature over the range 1000–2000 K, as demonstrated in a recent study on formaldehyde fluorescence in a CH_4/air diffusion flame [79]. In addition, the PAH fluorescence profiles typically extend over the entire fuel-rich region in these hydrocarbon diffusion flames, potentially leading to a considerable variation of the quenching rate with flame position. The quenching rate for electronically excited PAH molecules is sensitive to the local O_2 concentration, while N_2, CO_2 and H_2O are not expected to quench excited PAH at appreciable rates [64, 80]. Thus, the lifetime of the PAH fluorescence will vary depending upon the particular burner system and upon the spatial location of the fluorescence measurement. Gomez et al. [38] deduced an upper limit of 10 ns for the PAH fluorescence lifetime detected in the rich regions of diffusion flames for several fuels. Cignoli et al. [63] and Ni et al. [70] have reported longer lifetimes for PAH fluorescence in C_2H_4/air diffusion flames ($\sim$ 20 and 30 ns, respectively), indicative of the slow quenching rates expected

when O_2 concentrations are extremely low. In comparison, the fluorescence lifetimes of radicals such as H·, O:, and OH· are estimated to be less than 2 ns under our diffusion flame conditions [68, 71, 81].

Despite the potential pitfalls described above, several investigators have used PAH fluorescence intensities as direct measures of PAH concentrations. Prado et al. [21] reported a good correlation between the fluorescence intensity and PAH concentration profiles obtained by quartz microprobe sampling. This group also studied turbulent natural gas/air flames in industrial-scale burners and found a similar relationship between the fluorescence signals and PAH concentrations [82]. Ni et al. [70] employed fast detection (5 ns) to minimize the effects of collisional quenching on the quantum yield of PAH fluorescence and then interpreted PAH fluorescence intensities as indicators of soot precursor concentrations. However, as previously mentioned, the relative intensities of PAH fluorescence can be used as a quantitative gauge of PAH concentrations only to the extent that one can establish that the combustion conditions are identical in the different flames under consideration, i.e., that the local temperatures, collisional environments, and the identities of the fluorescing aromatics are the same. In recognition of the difficulties inherent in proving such close similarity, Kennedy [50] has coined the term "apparent concentration" in discussing relative PAH fluorescence intensities.

Effect of Combustion Conditions on PAH Fluorescence

Few prior investigations have discussed the influence of the local combustion conditions upon PAH fluorescence or directly compared intensities for different hydrocarbon fuels. Prado et al. [21] found that the PAH fluorescence signals excited at 488 nm in a CH_4/air diffusion flame correlated with the local equivalence ratio in the range of $\phi = \sim 1.3$–4.0. Similarly, Smyth et al. [4] observed that components of PAH fluorescence excited with both UV and visible light followed temperature isotherms in the 1300–1600 K range for a CH_4/air diffusion flame. Since temperature correlates with the mixture fraction (at least for lightly sooting fuels [83]), this is an equivalent result. Note that the concentrations of individual aromatic species do not correlate with the mixture fraction [4, 84]. Beretta et al. [56] found a fivefold increase in the PAH fluorescence intensities in an axisymmetric ethylene/air diffusion flame compared to a methane flame using excitation wavelengths of 250 and 436 nm. This agrees very well with our measurements (see Table 1).

Kennedy [50] burned ethane, propane, butane, ethylene, propylene, and acetylene in a Tsuji counterflow diffusion flame configuration, and monitored PAH fluorescence arising from pulsed excitation at 420 nm. Although fluorescence intensities were not reported for the different fuels, he did observe that the PAH fluorescence signals decreased with increasing velocity gradient (or decreasing residence time). In these measurements the variations in peak flame temperatures are expected to be small, since the strain rates under investigation were far from extinction conditions. Ethane exhibited the highest sensitivity to the imposed strain rate, followed by ethylene and then propylene. This order is the reverse of the relative sooting tendencies for these fuels [50]. Kennedy concluded that the variation of the PAH fluorescence intensity reflected the sensitivity of PAH formation to the imposed velocity gradient.

The enhanced PAH fluorescence intensities measured in the present study for the flickering vs steady flame conditions (Table 1) are consistent with Kennedy's observations. Kaplan et al. [85] have identified longer residence times as the key factor in their successful prediction of the enhanced soot concentrations produced in flickering vs steady CH_4/air flames [10, 12]. For example, the residence time in the soot growth region (i.e., the time between soot inception and the peak soot concentration) was computed to be three times longer (37 vs 13 ms) in the flickering flame compared to steady flame conditions [85]. Shaddix and Smyth [12, Table 1] observed that the relative enhancement of soot production in the flickering flames increased as the sooting tendency decreased. Similarly, the relative increase in the PAH fluorescence intensity for

the flickering flames is largest for methane. It appears that soot inception and growth occur so fast for a heavily sooting fuel that the added residence time in the flickering flames has less of an impact on overall soot production than for a more weakly sooting fuel. This same general behavior occurs for the intensity of the PAH fluorescence as well, perhaps reflecting the effect of PAH scavenging by high soot concentrations in the propane and ethylene flames.

The possible role of the molecules responsible for the PAH fluorescence in soot formation can be further examined in Fig. 10, which compares PAH fluorescence profiles in the steady flames (see Fig. 4) with those of the soot volume fraction [12]. Similar to the structure of the soot fields, the PAH fluorescence exhibits stronger annular signals for the more heavily sooting propane and ethylene fuels. Centerline soot production is greatest for methane relative to the annular region, and the corresponding PAH fluorescence is also relatively intense on the centerline. For all of the steady flames, the PAH fluorescence signals disappear as the soot volume fraction reaches its maximum values at $H = 65$, 40 and 35 mm above the burner for methane, propane, and ethylene, respectively (also see Fig. 4). Rapp and Santoro [86] reported the same trend for acetylene, diacetylene, and benzene concentrations above $H = 30$ mm in their axisymmetric, nonsmoking C_2H_4/air diffusion flame. They concluded that this depletion of intermediate hydrocarbons leads to the cessation of particle growth. The intensity of the PAH fluorescence behaves similarly, suggesting that the fluorescing molecules are involved in soot inception and/or growth. Another possible explanation for the disappearance of the PAH fluorescence signals is that the species responsible are oxidized. However, this is unlikely since PAH exhibit low diffusion velocities [74] and the PAH fluorescence signals at the centerline disappear well before the stoichiometric flame height is reached (the stoichiometric flame height should lie close to the luminous flame height [77, 84, 87]).

Figure 11 shows the evolution of the PAH fluorescence signal along the centerline of the steady flames, compared to our measurements of the soot volume fraction [12]. Note that in these plots there is a direct correlation between residence time and height above the burner, since the centerline coincides with a streamline. For each fuel the PAH fluorescence signal reaches a maximum value and starts to decrease just as soot production begins. The rise and fall of the PAH fluorescence and soot concentrations overlap most noticeably in the methane flame, while for the more heavily sooting fuels, propane and ethylene, the PAH fluorescence signal vanishes by the time the soot concentration reaches its maximum centerline value. The results presented in Fig. 11 lend support to the view that the fluorescing PAH species participate in soot production, if not in the early inception step [4] then later as growth species [47, 48, 51–54, 74]. Thermal decomposition of the aromatic species could also play a role in the disappearance of the PAH fluorescence. However, the centerline temperatures are quite different in regions where the PAH fluorescence signals decrease in the methane flame (1675–1850 K) vs the ethylene flame (1530–1580 K) [75]. The low temperatures at which the ethylene PAH fluorescence decreases indicate that thermal breakdown is not the dominant loss process. In addition, the narrow range of temperatures in the ethylene flame shows that the fall-off of the centerline signals is not controlled by the temperature dependence of the PAH fluorescence. Combined with the unlikelihood of PAH oxidation along the centerline discussed above, the disappearance of the PAH fluorescence is most probably caused by soot inception and growth. This close coupling of the PAH fluorescence to soot growth processes is most apparent for the steady propane and ethylene flames. In the case of methane the evolution of the PAH fluorescence occurs later in time along the centerline (see Fig. 11), such that PAH destruction via oxidation and thermal breakdown may also be significant.

Gomez et al. [38] also measured PAH fluorescence (excited at 460 nm) and soot scattering along the centerline of axisymmetric acetylene, 1-butene, 1,3-butadiene, and benzene diffusion flames burning at their respective smoke heights. Similar to our results for the propane and ethylene flames, they observed

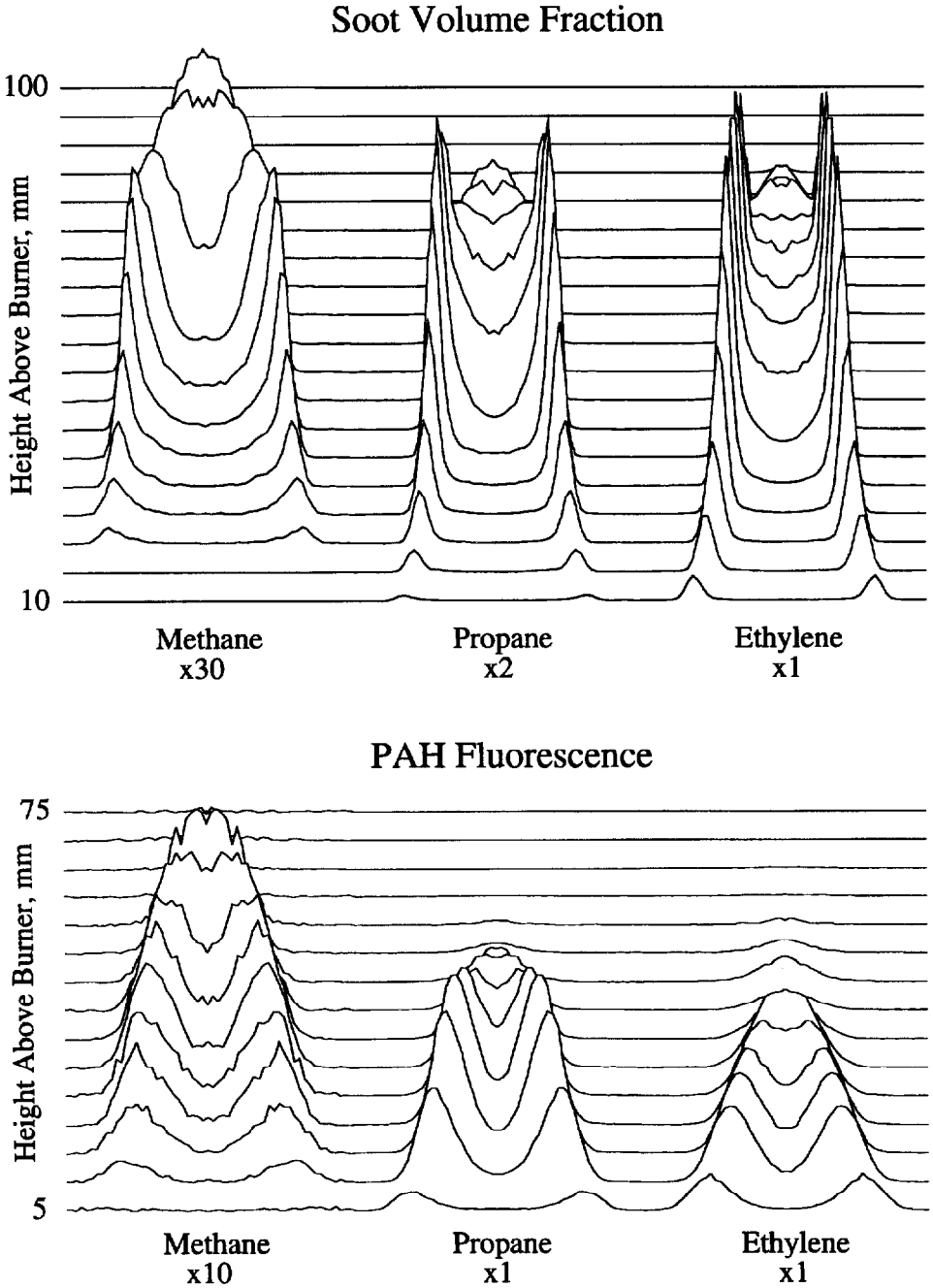

Fig. 10. Comparison of PAH fluorescence profiles in the steady flames (bottom; from Fig. 4) with those of the soot volume fraction (top; from Ref. 12). Note the indicated relative scalings within each data set; see also Table 1. The profiles extend from +7 to −7 mm radially for each flame and are shown every 5 mm in height above the burner, offset at each height for clarity.

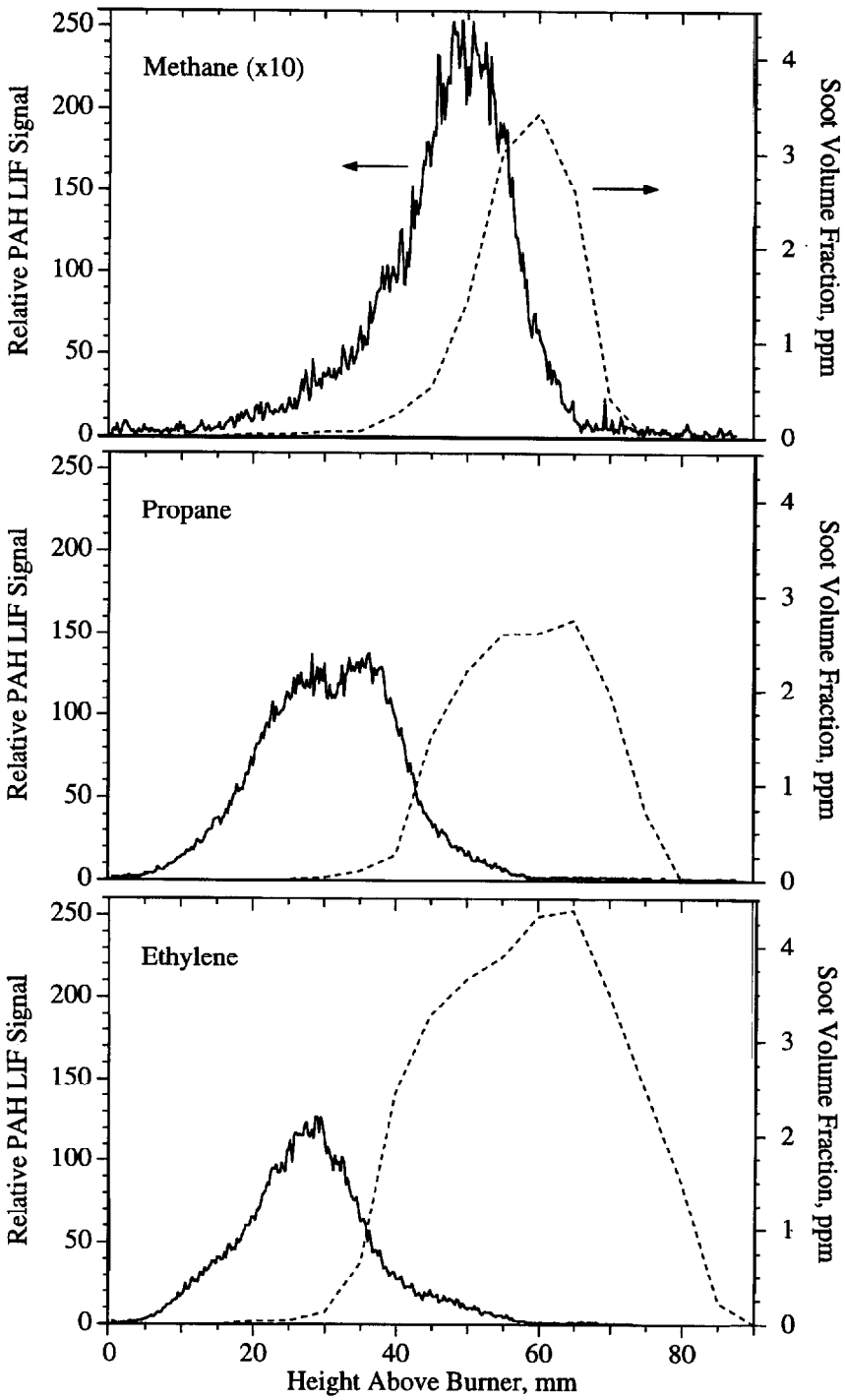

Fig. 11. Relative PAH fluorescence intensity (solid lines; scale at left) and quantitative soot concentrations (dotted lines; scale at right in ppm, 10^{-6}; see Ref. 12) along the centerline of the steady methane, propane, and ethylene flames. Note that the scaling of the PAH fluorescence and the soot concentrations for the methane flame is 10 × more sensitive than for propane and ethylene.

that the PAH fluorescence signals reached their maxima just as soot inception occurred and concluded that the PAH fluorescence is an indicator of soot inception sites. Santoro et al. [36] presented evidence linking PAH fluorescence to soot inception in ethylene diffusion flames by noting that the location of maximum visible PAH fluorescence coincides with a region where the soot number density increases rapidly. Recently, Vander Wal studied this same axisymmetric ethylene flame [44] and observed that along the centerline the PAH fluorescence signal decreases as soot concentrations rise, in agreement with our results presented in Fig. 11.

In the flickering flames the PAH fluorescence does not track the soot volume fraction closely (Fig. 5). For example, our earlier soot measurements in propane and ethylene flames revealed that flame clip-off leads to a burst of soot production near the base of the clipped flamelet [12], most likely due to higher temperatures in the rich interior region. This is not reflected in the PAH fluorescence signals at the same spatial location. In general, the PAH fluorescence signals are high in the clipped flamelets (Fig. 5), while the peak soot concentrations have stopped increasing [12], suggesting that simultaneous soot production and oxidation are occurring in these regions.

Visible Soot Luminosity

The most intense visible flame luminosity arises from soot particles at high temperatures, most likely in regions where vigorous soot oxidation is occurring. This interpretation is strongly supported by our measurements of OH· fluorescence and soot scattering [9–12]. Figure 12 compares visible emission images with those of two-dimensional laser-induced OH· fluorescence and soot scattering. In the lightly sooting methane flames, where radiation losses are small, the strongest luminosity is observed at the top of the steady flame (Fig. 6), while in the flickering flames the most intense signals are detected at the top and bottom of the clipped-off flamelet (Fig. 7). For the propane and ethylene flickering flames, the most intense visible emission occurs at the pinch-off location. Strong luminosity signals are also observed at the top of the lower flame (attached to the burner), as well as at the bottom of the clipped flamelet (Fig. 7). All of these regions of intense visible luminosity are where the OH· fluorescence and soot scattering signals lie immediately adjacent to one another or overlap, indicating active soot oxidation by OH· (Fig. 12). In contrast, at the locations of the highest soot concentrations (i.e., where the scattering signals are largest) there is a clear separation between the OH· layer and the soot zone. The weak visible luminosity shows that these regions are relatively cool. Soot breaks out at the top of the clipped propane and ethylene flamelets [12], and here OH· concentrations are small (Fig. 12). The visible luminosity is also weak, especially for the flickering ethylene flames, since temperatures and soot oxidation rates are low.

The only exceptions to this general picture of strong visible luminosity occurring where soot is being oxidized are the steady propane and ethylene flames. Radiation losses are large in these flames, giving much lower temperatures in the soot oxidation region (by ~ 300 K) than are measured for the steady methane flame [68, 75]. The result is that the strongest visible luminosity signals do not appear in the soot oxidation region for the steady propane and ethylene flames, but rather in the vicinity of the highest soot concentrations (Fig. 6).

In summary, intense visible flame luminosity is an excellent indicator of regions where soot oxidation is active, while being a poor measure of the total soot radiation. Visible flame emission thus complements soot volume fraction measurements by identifying regions of soot destruction.

CONCLUSIONS

PAH fluorescence signals excited at both UV and visible wavelengths in steady and flickering methane, propane, and ethylene diffusion flames are strongest for the propane flames, whereas the peak soot concentrations are largest in the ethylene flames. Methane flames exhibit by far the smallest PAH fluorescence signals and soot concentrations. Although the relative PAH fluorescence intensities do not quantitatively reflect PAH concentrations,

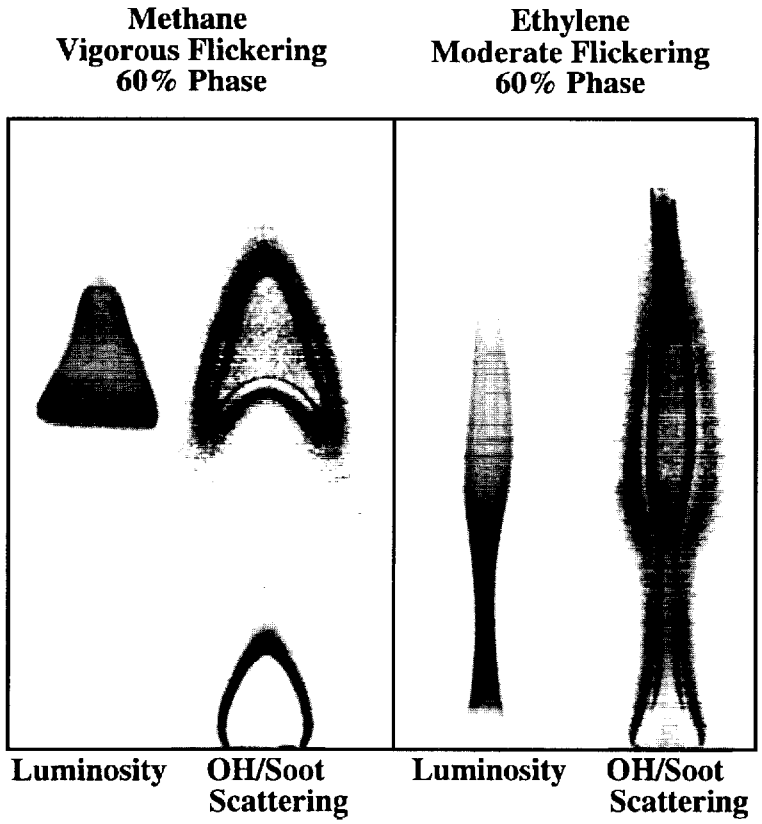

Fig. 12. Comparison of the visible flame luminosity images (left) with those of combined OH· and soot scattering (right) for selected flickering flame conditions (also see Fig. 7).

these results suggest that the highest PAH levels occur in the propane flames. Analysis of the steady flame results indicates that rapid soot inception and growth in the ethylene flames may act to limit PAH populations as the aromatic species participate in soot production.

In the steady flames the PAH fluorescence signals first appear in an annular region just to the rich side of the high-temperature reaction zone, and soot inception occurs at the interface between the fluorescing PAH and the location of peak radical concentrations. Along the centerline of these flames the PAH fluorescence reaches a maximum near the location of soot inception and then falls as the soot concentrations increase. These observations strongly implicate the fluorescing molecules in soot inception and growth, since PAH oxidation and thermal decomposition cannot readily account for the disappearance of the PAH fluorescence.

PAH fluorescence increases for all fuels in the flickering flames, where longer residence times favorable for molecular growth and soot production are available compared to steady flame conditions. The relative enhancement of the PAH fluorescence is largest for methane, which also exhibits the greatest relative increase in soot concentrations for flickering flames.

Visible flame luminosity monitored at a single bandpass is a useful indicator of high-temperature soot but is not a good measure of the total radiation from soot particles. For flickering flame conditions, intense luminosity is detected only where significant OH· concentrations overlap the soot layer, i.e., where active

soot oxidation is occurring. Although the largest soot concentrations are present high in the flickering propane and ethylene flames, visible luminosity signals are weak at these locations since OH· concentrations are collapsing as soot breaks out.

This work was supported in part by the Basic Research Group of the Gas Research Institute, under Contract 5093-260-2676.

REFERENCES

1. Hamins, A., Yang, J. C., and Kashiwagi, T., *Twenty-Fourth Symposium (International) on Combustion*, The Combustion Institute, Pittsburgh, 1992, p. 1695, and references therein.
2. Cetegen, B. M., and Ahmed, T. A., *Combust. Flame* 93:157 (1993).
3. Glassman, I., *Twenty-Second Symposium (International) on Combustion*, The Combustion Institute, Pittsburgh, 1988, p. 295, and references therein.
4. Smyth, K. C., Miller, J. H., Dorfman, R. C., Mallard, W. G., and Santoro, R. J., *Combust. Flame* 62:157 (1985).
5. Kent, J. H., and Honnery, D., *Combust. Sci. Technol.* 54:383 (1987).
6. Kent, J. H., and Honnery, D. R., *Combust. Flame* 79:287 (1990).
7. Moss, J. B., Stewart, C. D., and Syed, K. J., *Twenty-Second Symposium (International) on Combustion*, The Combustion Institute, Pittsburgh, 1988, p. 413.
8. Sivathanu, Y. R., and Gore, J. P., Central and Eastern States Sections Meeting of the Combustion Institute, March, 1993, Paper #123.
9. Smyth, K. C., Harrington, J. E., Johnsson, E. L., and Pitts, W. M., *Combust. Flame* 95:229 (1993).
10. Shaddix, C. R., Harrington, J. E., and Smyth, K. C., *Combust. Flame* 99:723 (1994); 100:518 (1995).
11. Harrington, J. E., Shaddix, C. R., and Smyth, K. C., *SPIE International Symposium on Laser Diagnostics in Combustion* (1994), Vol. 2124, Paper #20.
12. Shaddix, C. R., and Smyth, K. C., *Combust. Flame* 107:418 (1996).
13. D'Alessio, A., Di Lorenzo, A., Borghese, A., Beretta, F., and Masi, S., *Sixteenth Symposium (International) on Combustion*, The Combustion Institute, Pittsburgh, 1977, p. 695.
14. Müller-Dethlefs, K., Ph.D. Dissertation, Imperial College, London, 1979.
15. Haynes, B. S., Jander, H., and Wagner, H. Gg., *Ber. Bunsenges. Phys. Chem.* 84:585 (1980).
16. D'Alessio, A., in *Particulate Carbon: Formation During Combustion* (D. C. Siegla and G. W. Smith, Eds.), Plenum, New York, 1981, p. 207.
17. Crittenden, B. D., and Long, R., *Combust. Flame* 20:359 (1973).
18. Hamins, A., Anderson, D. T., and Miller, J. H., *Combust. Sci. Technol.* 71:175 (1990).
19. D'Alessio, A., D'Anna, A., D'Orsi, A., Minutolo, P., Barbella, R., and Ciajolo, A., *Twenty-Fourth Symposium (International) on Combustion*, The Combustion Institute, Pittsburgh, 1992, p. 973.
20. Ciajolo, A., D'Anna, A., and Barbella, R., *Combust. Sci. Technol.* 100:271 (1994).
21. Prado, G., Garo, A., Ko, A., and Sarofim, A., *Twentieth Symposium (International) on Combustion*, The Combustion Institute, Pittsburgh, 1984, p. 989.
22. Beretta, F., D'Alessio, A., D'Orsi, A., and Minutolo, P., *Combust. Sci. Technol.* 85:455 (1992).
23. Parker, W. G., and Wolfhard, H. G., *J. Chem. Soc.* p. 2038 (1950).
24. Wolfhard, H. G., and Parker, W. G., *Proc. Phys. Soc. London, Section A* 65:2 (1952).
25. Jessen, P. F., and Gaydon, A. G., *Twelfth Symposium (International) on Combustion*, The Combustion Institute, Pittsburgh, 1969, p. 481.
26. Laud, B. B., and Gaydon, A. G., *Combust. Flame* 16:55 (1971).
27. Harvey, R., and Jessen, P. F., *Nature* 241:102 (1973).
28. Prado, G. P., and Howard, J. B., *Adv. Chemistry Ser.*, J. T. Zung, Ed., 166:153 (1978).
29. Cincotti, V., D'Alessio, A., Menna, P., and Venitozzi, C., *La Rivista dei Combustibili* 35:59 (1981).
30. Di Lorenzo, A., D'Alessio, A. Cincotti, V., Masi, S., Menna, P., and Venitozzi, C., *Eighteenth Symposium (International) on Combustion*, The Combustion Institute, Pittsburgh, 1981, p. 485.
31. Miller, J. H., Mallard, W. G., and Smyth, K. C., *Seventh International Symposium on Polycyclic Aromatic Hydrocarbons*, Batelle Press, Columbus, OH, 1982, p. 905.
32. Andreussi, P., Barbieri, B., and Petarca, L., *Combust. Sci. Technol.* 49:123 (1986).
33. Weiner, A. M., and Harris, S. J., *Combust. Flame* 77:261 (1989).
34. D'Alessio, A., Gambi, G., Minutolo, P., Russo, S., and D'Anna, A., *Twenty-Fifth Symposium (International) on Combustion*, The Combustion Institute, Pittsburgh, 1994, p. 645.
35. Haynes, B. S., and Wagner, H. Gg., *Ber. Bunsenges., Phys. Chem.* 84:499 (1980).
36. Santoro, R. J., Semerjian, H. G., and Dobbins, R. A., *Combust. Flame* 51:203 (1983).
37. Santoro, R. J., and Semerjian, H. G., *Twentieth Symposium (International) on Combustion*, The Combustion Institute, Pittsburgh, 1984, p. 997.
38. Gomez, A., Littman, M. G., and Glassman, I., *Combust. Flame* 70:225 (1987).
39. Ray, S. K., and Long, R., *Combust. Flame* 8:139 (1964).
40. Homann, K. H., and Wagner, H. Gg., *Eleventh Symposium (International) on Combustion*, The Combustion Institute, Pittsburgh, 1967, p. 371.
41. Tompkins, E. E., and Long, R., *Twelfth Symposium (International) on Combustion*, The Combustion Institute, Pittsburgh, 1969, p. 625.

42. Lam, F. W., Howard, J. B., and Longwell, J. P., *Twenty-Second Symposium (International) on Combustion*, The Combustion Institute, Pittsburgh, 1988, p. 323.
43. Allen, M. G., McManus, K. R., Sonnenfroh, D. M., and Paul, P. H., *Appl. Opt.* 34:6287 (1995).
44. Vander Wal, R. L., *Combust. Sci. Technol.* 118:343 (1996).
45. Bittner, J. D., and Howard, J. B., *Eighteenth Symposium (International) on Combustion*, The Combustion Institute, Pittsburgh, 1981, p. 1105.
46. Smedley, J. M., Williams, A., and Bartle, K. D., *Combust. Flame* 91:71 (1992).
47. McKinnon, J. T., and Howard, J. B., *Twenty-Fourth Symposium (International) on Combustion*, The Combustion Institute, Pittsburgh, 1992, p. 965.
48. McKinnon, J. T., Meyer, E., and Howard, J. B., *Combust. Flame* 105:161 (1996).
49. Petarca, L., and Marconi, F., *Combust. Flame* 78:308 (1989).
50. Kennedy, I. M., *Combust. Sci. Technol.* 59:107 (1988).
51. Mukherjee, J., Sarofim, A. F., and Longwell, J. P., *Combust. Flame* 96:191 (1994).
52. Marr, J. A., Giovane, L. M., Longwell, J. P., Howard, J. B., and Lafleur, A. L., *Combust. Sci. Technol.* 101:301 (1994).
53. Hepp, H., Siegmann, K., and Sattler, K., *Chem. Phys. Lett.* 233:16 (1995).
54. Siegmann, K., Hepp, H., and Sattler, K., *Combust. Sci. Technol.* 109:165 (1995).
55. Miller, J. H., Mallard, W. G., and Smyth, K. C., Eastern States Section Meeting of the Combustion Institute, October 1981, Paper #39.
56. Beretta, F., Cincotti, V., D'Alessio, A., and Menna, P., *Combust. Flame* 61:211 (1985).
57. Fujiwara, K., Omenetto, N., Bradshaw, J. B., Bower, J. N., and Winefordner, J. D., *Appl. Spectrosc.* 34:85 (1980).
58. Jagoda, I. J., Prado, G., and Lahaye, J., *Combust. Flame* 37:261 (1980).
59. Bard, S., and Pagni, P. J., *J. Quantitative Spectrosc. Radiat. Transf.* 25:453 (1981).
60. Toqan, M., Farmayan, W. F., Beér, J. M., Howard, J. B., and Teare, J. D., *Twentieth Symposium (International) on Combustion*, The Combustion Institute, Pittsburgh, 1984, p. 1075.
61. Coe, D. S., Haynes, B. S., and Steinfeld, J. I., *Combust. Flame* 43:211 (1981).
62. Miller, J. H., Mallard, W. G., and Smyth, K. C., *Combust. Flame* 47:205 (1982).
63. Cignoli, F., Benecchi, S., and Zizak, G., *Appl. Opt.* 33:5778 (1994).
64. Coe, D. S., and Steinfeld, J. I., *Chem. Phys. Lett.* 76:485 (1980).
65. Peterson, D. L., Lytle, F. E., and Laurendeau, N. M., *Opt. Lett.* 11:345 (1986); *Appl. Opt.* 27:2768 (1988).
66. Everest, D. A., Shaddix, C. R., and Smyth, K. C., *Twenty-Sixth Symposium (International) on Combustion*, The Combustion Institute, Pittsburgh, p. 1161.
67. Pitts, W. M., *Twenty-Sixth Symposium (International) on Combustion*, The Combustion Institute, Pittsburgh, p. 1171.
68. Puri, R., Moser, M., Santoro, R. J., and Smyth, K. C., *Twenty-Fourth Symposium (International) on Combustion*, The Combustion Institute, Pittsburgh, 1992, p. 1015.
69. Zhang, J., and Megaridis, C. M., Central States Section Meeting of the Combustion Institute, May, 1996, Paper #22; *Combust. Flame*, in press.
70. Ni, T., Gupta, S. B., and Santoro, R. J., *Twenty-Fifth Symposium (International) on Combustion*, The Combustion Institute, Pittsburgh, 1994, p. 585.
71. Smyth, K. C., Tjossem, P. J. H., Hamins, A., and Miller, J. H., *Combust. Flame* 79:366 (1990), and references therein.
72. Smyth, K. C., and Everest, D. A., *Twenty-Sixth Symposium (International) on Combustion*, The Combustion Institute, Pittsburgh, p. 1385.
73. Santoro, R. J., Yeh, T. T., Horvath, J. J., and Semerjian, H. G., *Combust. Sci. Technol.* 53:89 (1987).
74. Miller, J. H., Mallard, W. G., and Smyth, K. C., *Twenty-First Symposium (International) on Combustion*, The Combustion Institute, Pittsburgh, 1986, p. 1057.
75. Richardson, T. F., and Santoro, R. J., personal communication, 1993.
76. Pearse, R. W. B., and Gaydon, A. G., *The Identification of Molecular Spectra*, 4th ed., Chapman and Hall, London, 1976.
77. Puri, R., Santoro, R. J., and Smyth, K. C., *Combust. Flame* 97:125 (1994); Erratum, *Combust. Flame* 102:226 (1995).
78. Senkan, S., and Castaldi, M., *Combust. Flame* 107:141 (1996).
79. Harrington, J. E., and Smyth, K. C., *Chem. Phys. Lett.* 202:196 (1993).
80. Whitaker, T. J., and Bushaw, B. A., *J. Phys. Chem.* 85:2180 (1981).
81. Smyth, K. C., and Tjossem, P. J. H., *Twenty-Third Symposium (International) on Combustion*, The Combustion Institute, Pittsburgh, 1990, p. 1829.
82. Thijssen, J. H., Toqan, M. A., Beér, J. M., and Sarofim, A. F., *Combust. Sci. Technol.* 90:101 (1993).
83. Norton, T. S., Smyth, K. C., Miller, J. H., and Smooke, M. D., *Combust. Sci. Technol.* 90:1 (1993).
84. Saito, K., Williams, F. A., and Gordon, A. S., *J. Heat Transfer* 108:640 (1986).
85. Kaplan, C. R., Shaddix, C. R., and Smyth, K. C., *Combust. Flame* 106:392 (1996).
86. Rapp, D. C., and Santoro, R. J., Spring Meeting of the Western States Section of the Combustion Institute, March, 1994, Paper #94-052; Rapp, D. C., Ph.D. thesis, Department of Mechanical Engineering, The Pennsylvania State University, 1996.
87. Mitchell, R. E., Sarofim, A. F., and Clomburg, L. A., *Combust. Flame* 37:227 (1980).

Received 29 July 1996; accepted 12 February 1997